J Sol-Gel Sci Technol (2009) 52:228–234
DOI 10.1007/s10971-009-2032-0

ORIGINAL PAPER

Effect of post-annealing on the band gap of sol–gel prepared nano-crystalline $Mg_xZn_{1-x}O$ ($0.0 \leq x \leq 0.3$) thin films

S. R. Meher · Kuyyadi P. Biju · Mahaveer K. Jain

Received: 29 January 2009 / Accepted: 18 June 2009 / Published online: 6 July 2009
© Springer Science+Business Media, LLC 2009

Abstract Polycrystalline $Mg_xZn_{1-x}O$ (MZO) thin films on glass substrates were prepared by sol–gel method. All the films retained the hexagonal wurtzite structure of ZnO. The band gap values determined from transmission spectra were found to be smaller than the values obtained from Vegard's law for the as-deposited MZO films. For the films with $x = 0.1$, 0.2 and 0.3, the band gap blue-shifted initially and then red-shifted with increase in the annealing temperature. The reason for this anomalous shift in the band gap is attributed to the proper substitution of Mg atoms into the Zn lattice sites after a certain critical annealing temperature.

Keywords MgZnO · Sol–gel · Thin film · Annealing · Band gap

1 Introduction

In the recent past, ZnO has been considered as one of the most promising candidates for development of short wavelength optoelectronic devices because of its wide band gap ($E_g = 3.3$ eV) and a large exciton binding energy ($\sim$60 meV). Optical band gap of ZnO can be enhanced by alloying it with Mg. Ohtomo et al. [1] have successfully tailored the band gap of $Mg_xZn_{1-x}O$ (MZO) ternary alloy films from 3.3 to 4.0 eV with Mg concentration increased up to $x = 0.33$. The MZO alloy films have often been used as a suitable barrier layer for ZnO laser diodes [2] and have got potential applications in solar-blind ultraviolet (UV) detectors [3]. Again, ZnO/MgZnO based heterostructures have received a great deal of attention due to their potential applications in optoelectronic devices in the blue-UV region of the spectrum [4–6]. The ionic radii of Mg^{2+} (0.78 Å) and Zn^{2+} (0.83 Å) are nearly equal [7]. As a result, very little lattice distortion can be caused when Zn is replaced by Mg. But, the higher energy level of Mg 3*s* orbital (as compared to Zn 4*s* orbital) pushes the conduction band edge of ZnO upwards. As a result of this, the band gap of the MZO alloy system is widened markedly.

MZO films have been grown by several techniques such as metal-organic vapour phase epitaxy (MOVPE) [8], molecular beam epitaxy (MBE) [9], RF magnetron co-sputtering [10], reactive electron beam evaporation deposition) [11], electrophoretic deposition (EPD) [12], pulsed laser deposition (PLD) [1, 13, 14], sol–gel [15], etc. According to the binary phase diagram, the solid solubility of MgO in a ZnO matrix is $\sim$4 at.% [16]. But, this solubility limit is found to be largely dependent on the deposition techniques and processing parameters. PLD grown films have shown a solubility limit of 33–36 at.% where as, an enhanced solubility of $\sim$49 at.% has been reported for MOVPE grown films. The enhancement in the solubility limit of MZO alloy system might be explained in terms of a non-thermal equivalent nature of the above mentioned growth techniques. Among all the deposition techniques, sol–gel has got certain distinct advantages in making alloy oxides such as easy and cheap operation, excellent compositional control and more importantly the ability to achieve atomic scale mixing of individual components. Some properties of MZO alloy films prepared by sol–gel technique have been studied earlier [15, 17–19]. But, very little work has been done on the effect of post annealing temperature on the band gap of sol–gel derived MZO alloy films.

S. R. Meher (✉) · K. P. Biju · M. K. Jain
Department of Physics, Indian Institute of Technology Madras, Chennai 600036, India
e-mail: samir@physics.iitm.ac.in

In the present work, MZO films with different Mg compositions ($x = 0.0$, 0.05, 0.1, 0.2, and 0.3) were prepared by sol–gel method. The effect of post-annealing on the band gap of these films has been studied. The reason for the experimental band gap of as-deposited films being lower than the values obtained from the Vegard's law has also been discussed.

2 Experimental procedure

The sol was prepared by dissolving $Zn(CH_3COOH)_2{\cdot}2H_2O$ and $Mg(CH_3COOH)_2{\cdot}4H_2O$ in isopropyl alcohol with monoethanolamine ($NH_2CH_2CH_2OH$; MEA) acting as the sol-stabilizer. The molar ratio of MEA to total metal ion concentration was kept to 1.0. The Mg content, $x = [Mg^{2+}]/([Mg^{2+}]+[Zn^{2+}])$ was varied from 0.0 to 0.3 keeping the total metal ion concentration fixed at 0.3 M. The resultant solution was stirred at room temperature for 5 h to yield a homogeneous solution. The sol was kept at room temperature for 24 h before being spin coated on glass substrates at a spinning speed of 3,000 rpm for 30 s. Twelve layers of the films were coated in order to obtain a thickness of ~400 nm measured using the spectrophotometer (Filmetrics F20). After coating each layer, the films were pre-heated at a temperature of 300 °C for 5 min in air. The structural properties of the films were determined using Phillips X'Pert Pro X-ray diffractometer with a Cu Kα radiation. The surface morphology was studied using Digital Instruments Nanoscope IV atomic force microscope (AFM) in contact mode. The transmittance spectra in the wavelength range 300–2,000 nm were recorded using a Jasco UV-VIS-NIR spectrophotometer. The photoluminescence (PL) spectra were taken with a Jobin Yvon Flurolog-3-11 spectroflurometer for which a 450 W Xe lamp was used as the excitation source. For all the samples the emission spectra were taken at an excitation wavelength of 270 nm. The photoresponse measurements were performed using a Keithley source measure unit (model-238). The photocurrents were measured at 10 V bias under ultraviolet (UV) illumination by a 6 W mercury lamp with central wavelength of 352 nm.

3 Results and discussion

Figure 1a shows the X-ray diffraction (XRD) pattern for the films annealed at 550 °C. All the films retain the hexagonal wurtzite structure of ZnO, indicating that Mg acts as a substitutional impurity in ZnO. The average crystallite size (D) and lattice strain (ε) were calculated using Scherrer's semi-empirical formula

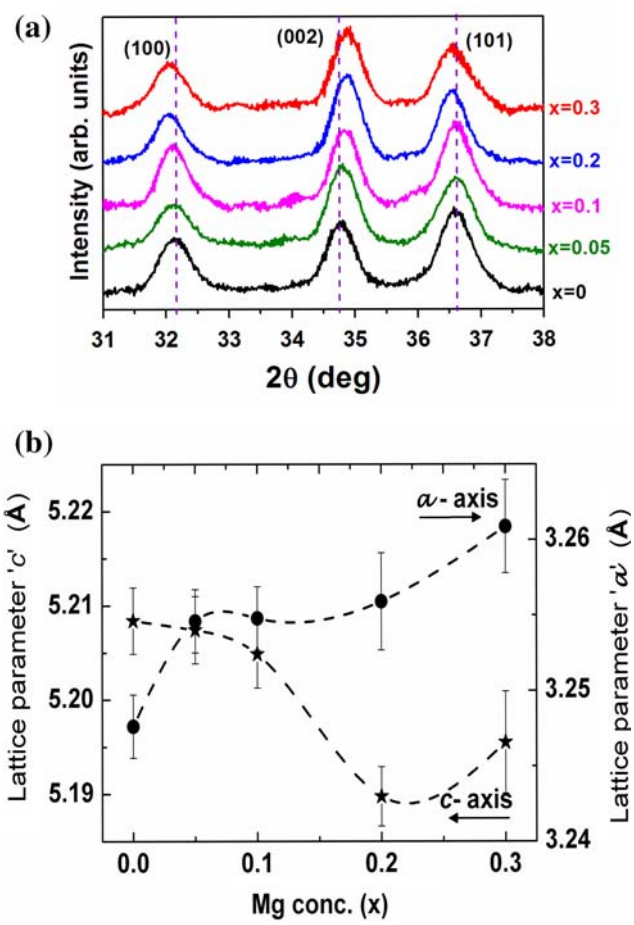

Fig. 1 **a** XRD pattern of MZO thin films annealed at 550 °C. **b** Change in lattice constant of MZO thin films with Mg concentration. (*Dotted line* drawn is only a guide line to the eye)

$$D = \frac{0.9\lambda}{\beta \cos\theta} \tag{1}$$

$$\varepsilon = \frac{\beta}{4 \tan\theta} \tag{2}$$

for the (002) orientation, where, $\lambda = 1.54$ Å and $\beta = B - b$ (B being the observed FWHM and b is the instrument function determined from the monocrystalline silicon diffraction line).

The average crystallite size and the lattice strain for the MZO alloy films at different annealing temperatures are listed in Table 1. We can see that the average crystallite size for all the samples increases from 10 to 18 nm with increase in the annealing temperature from 300 to 550 °C. The lattice strain is found to be decreasing with annealing temperature for all the samples. The structural evolution in the MZO films is first recognized from the positions of (100) and (002) peaks (Fig. 1b). The (100) and (002) diffraction peaks are shifted towards lower and higher angles respectively, as x increases. In other words the hexagonal lattice constant a increases and c decreases with the progress of

Table 1 Average crystallite size (D) and lattice strain (ε) of MZO alloy films at different annealing temperatures

Mg concentration (x)	Annealing temperature (°C)							
	300		400		500		550	
	D (nm)	ε (%)	D (nm)	ε (%)	D (nm)	ε (%)	D (nm)	ε (%)
0.0	10.2	1.12	12.9	0.98	13.1	0.95	15.0	0.85
0.05	9.8	1.59	10.4	1.37	15.7	0.80	16.2	0.80
0.1	9.6	1.40	9.7	1.27	14.1	0.84	16.2	0.78
0.2	9.8	1.38	10.0	1.22	16.3	0.78	18.9	0.73
0.3	9.7	1.34	9.9	1.24	14.7	0.88	17.7	0.67

Mg substitution in ZnO as shown in Fig. 1b. The a and c parameters (up to $x = 0.2$) follow approximately, the relationships: $a(\text{Å}) = 3.2499\ (\pm 0.0016) + 0.0417\ (\pm 0.0181)\ x$ and $c(\text{Å}) = 5.2110\ (\pm 0.0027) - 0.0983\ (\pm 0.0223)\ x$. Similar trend is also reported by Kim et al. [20] for polycrystalline MZO powder sample prepared by oxalate based co-precipitation method. An increase in a-axis and decrease in c-axis length with increasing Mg content has also been reported by Ohtomo et al. [1] for MZO films prepared on sapphire substrates by PLD technique. This is a general trend found in the binary wurtzite family. The c/a ratio is strongly correlated with the electronegativity difference [21]. The compounds with greater electronegativity difference show larger departure from the ideal c/a ratio i.e., 1.633. These distortions are caused by the long range polar interactions. In the presence of ionic charges, the crystal gains polar energy. Hence, in the MZO alloy films the increased ionicity brought by Mg^{2+} is responsible for the compression of c-axis and the expansion of a-axis. The (200) diffraction peak corresponding to the cubic phase of MgO (not shown here) starts to appear for $x = 0.3$ film annealed at 450 °C. From this we can infer that the solubility limit of MgO in ZnO hexagonal wurtzite phase lies between 20 and 30 at.%.

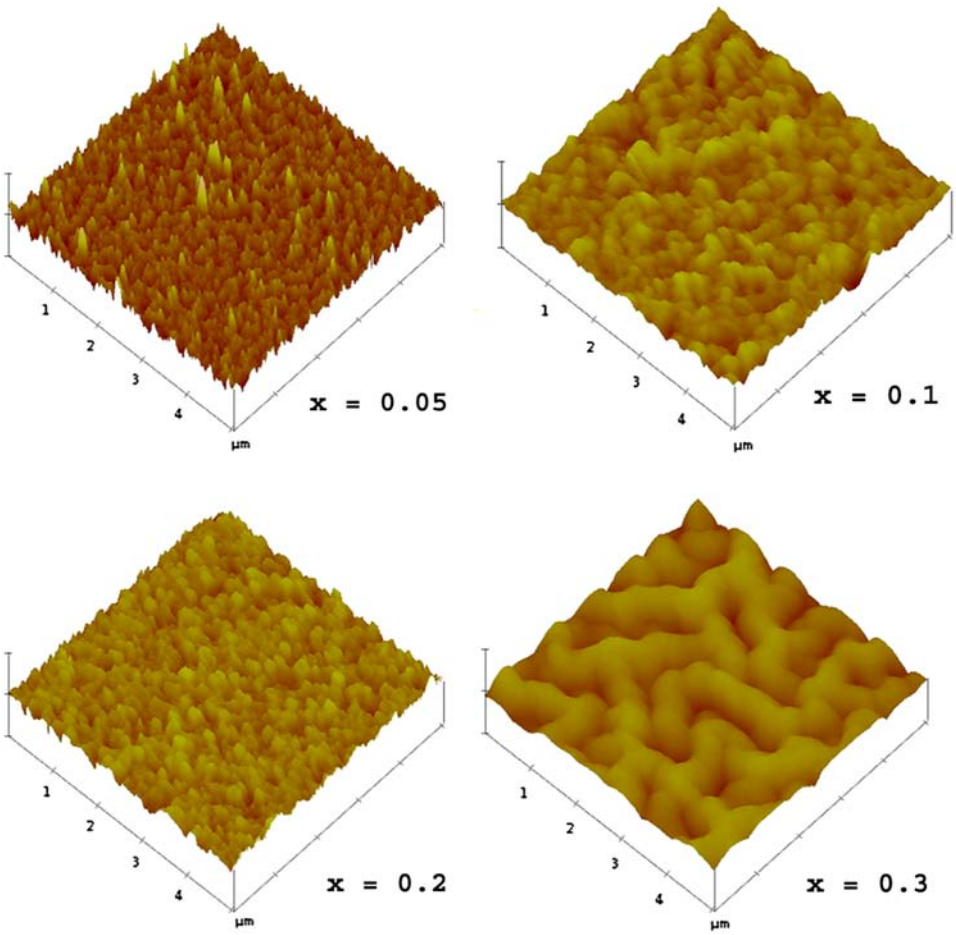

Fig. 2 AFM images (5 µm × 5 µm) of MZO alloy films annealed at 500 °C

AFM images of the MZO alloy films annealed at 500 °C are shown in Fig. 2. All the films up to $x = 0.2$, show granular structure where as noodle shaped structure evolve for $x = 0.3$ film. With the progress of Mg substitution, the surface of the films becomes rougher.

Figure 3a shows the transmission spectra of MZO alloy films annealed at 550 °C. All the films are highly transparent (80–90%) in the VIS-NIR region. The energy band gap values were calculated using the relations given below [22]:-

$$\alpha = \frac{2.303\ \log(1/T)}{d} \tag{3}$$

$$\alpha h\nu = A(h\nu - E_g)^{1/2} \tag{4}$$

where, α is the absorption coefficient, T is the transmittance, d is the film thickness, E_g is the direct band gap energy and A is a constant. So, the energy band gap values can be determined by plotting the squared absorption coefficient (α^2) as a function of photon energy ($h\nu$) and linearly extrapolating to $\alpha = 0$ (Fig. 3b). For the as-deposited films, the band gap values determined are found to be smaller than the values obtained from Vegard's law as shown in the Fig. 4 (E_g of wurtzite MgO at room temperature is 5.20 eV [23]):-

$$E_g(\mathrm{MZO}) = 1.90x + 3.30\,\mathrm{eV} \tag{5}$$

This difference might be due to the random distribution of Mg in as-deposited MZO alloy films. The Mg atoms might be incorporated at the interstitial sites and the grain boundaries. In order to verify this, all the films were annealed for 2 h in air at different temperatures. For the films with $x = 0.0$ and 0.05, there is a slight decrease in the band gap with annealing temperature which is mainly due to the lattice strain and quantum confinement effect (Fig. 5). The energy shift induced by the quantum confinement effect (ΔE_{QC}) can be calculated by the following equation [24]:-

$$\Delta E_{QC} = \frac{\hbar^2\pi^2}{2D^2\mu} - \frac{1.8e^2}{\varepsilon D} \tag{6}$$

where, D is the grain size, $\frac{1}{\mu} = \frac{1}{m_e} + \frac{1}{m_h}$ (m_e and m_h being the effective electron and hole mass respectively) and ε is the dielectric constant. Here, we have used the values for pure ZnO. For ZnO, the effective masses of electrons and holes are $0.38m_o$ and $1.80m_o$, respectively [25] (m_o being the mass of electron at rest) and $\varepsilon = 8.75$ [26]. From Eq. 6, the values of ΔE_{QC} are calculated to be 16 and 14 meV (for

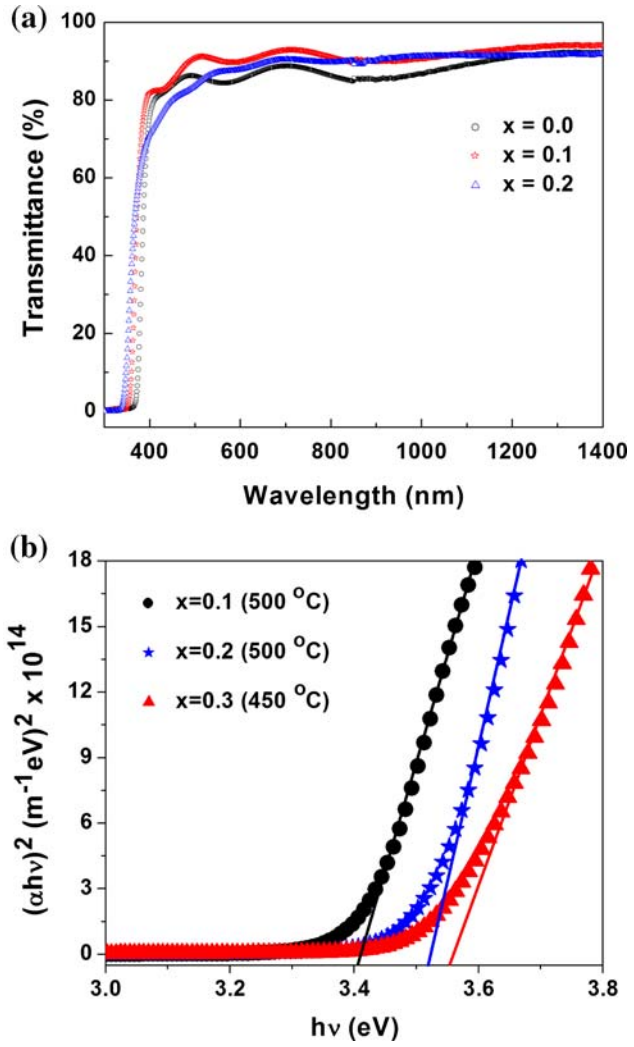

Fig. 3 **a** Transmission spectra of MZO thin films annealed at 550 °C. **b** Squared absorption coefficient plots for the samples annealed at 500 °C ($x = 0.1$, 0.2) and 450 °C ($x = 0.3$)

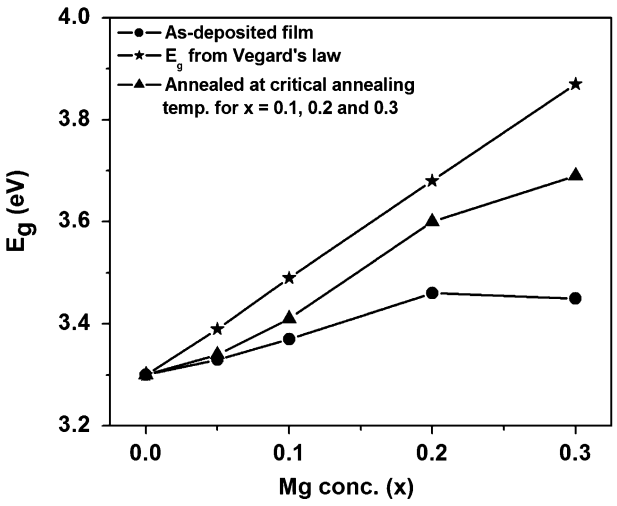

Fig. 4 Comparison of energy band gap values obtained from Vegard's law and transmission spectra for the as-deposited films and the films annealed at their respective critical annealing temperatures

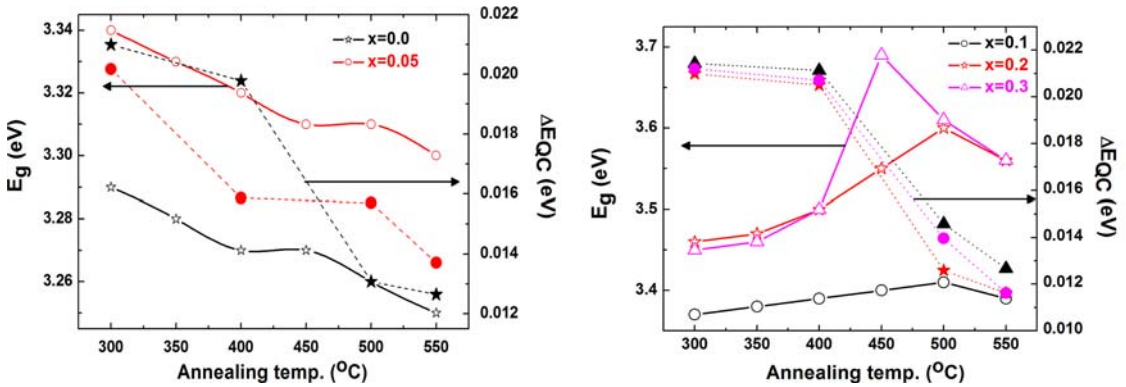

Fig. 5 Variation of energy band gap and quantum confined energy shift with annealing temperature for MZO thin films with different Mg contents

$x = 0.0$) and 13 and 12 meV (for $x = 0.05$) for the samples annealed at 500 and 550 °C, respectively. This quantum confined energy shift accounts only for 1/10th of the observed blue-shift. The remaining shift can be attributed to the relaxation of built-in tensile lattice strain in the films with annealing temperature.

However, for the films with higher Mg concentration ($x = 0.1$, 0.2, 0.3), the band gap blue-shifted initially and then red-shifted with increase in the annealing temperature (Fig. 5). So, there exists a certain critical annealing temperature up to which the band gap increases with increase in the annealing temperature and decreases thereafter. The band gap shifting to higher energy can be attributed to Mg atoms being induced to the lattice points. For $x = 0.1$ and 0.2 films, the band gap started to decrease after 500 °C due to lattice strain and quantum confinement effect which start to dominate after this critical annealing temperature for these films. In other words, we can say that for the films with $x = 0.1$ and 0.2, all the Mg atoms are properly induced to the lattice points at 500 °C. But, for $x = 0.3$ film, the band gap started to decrease after a lower critical annealing temperature of 450 °C. This may be due to the poor bonding of Mg atoms into MZO alloy films at higher Mg concentrations [27]. This fact has also been verified from the XRD pattern for which no real shift is observed for (100) and (002) diffraction peaks between $x = 0.2$ and $x = 0.3$ films annealed at 550 °C. So, we can infer that there is a loss of Mg atoms from the $x = 0.3$ MZO film after the critical annealing temperature of 450 °C leading to a decrease in the band gap.

Figure 6a shows the PL spectra for the MZO films annealed at 550 °C. For all the films, strong UV emission corresponding to near band edge (NBE) is observed. A broad blue emission at around 420 nm is also observed for all the films which is primarily due to the transitions of

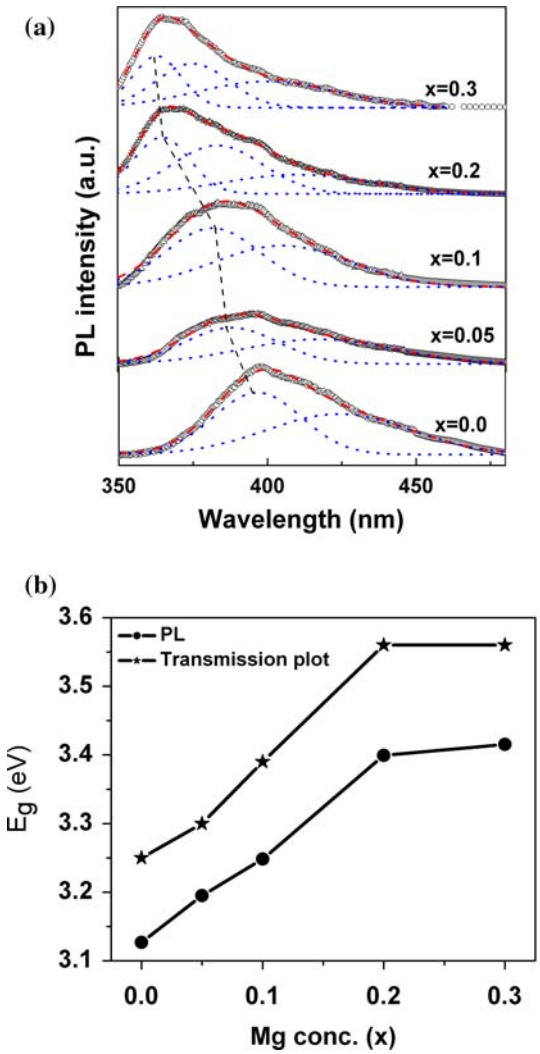

Fig. 6 **a** PL spectra of MZO alloy films annealed at 550 °C. **b** Energy band gap and PL peak energies as a function of Mg content for the films annealed at 550 °C

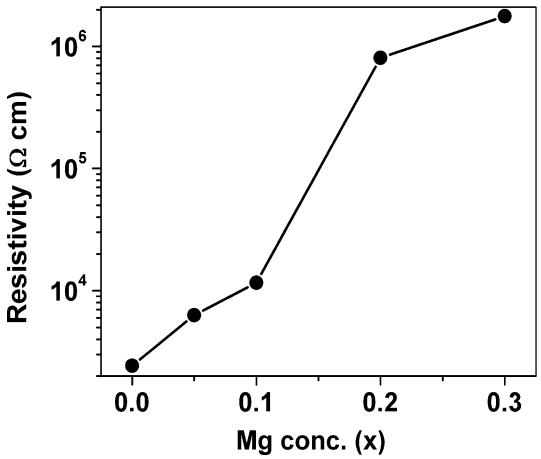

Fig. 7 Resistivity of MZO alloy films annealed at 500 °C

electrons from shallow donor of oxygen vacancy and zinc interstitials to the valence band [28]. However, for the films with $x = 0.2$ and 0.3, an additional peak at around 388 nm is seen which is attributed to the defect centers (such as F^{+} centers) in MgO [29]. The band gap values obtained from the band edge emission of PL spectra are in good agreement (Fig. 6b) with the values deduced from transmission spectra. Here also, we can observe that the band gap values for $x = 0.2$ and $x = 0.3$ films annealed at 550 °C are nearly the same confirming the fact that there is a loss of Mg atoms from the $x = 0.3$ film at higher annealing temperatures.

The resistivity of the MZO alloy films annealed at 500 °C (Fig. 7) increases by an order of $\sim 10^3$ with the increase in the Mg concentration which is mainly due to the widening of the energy band gap with more and more Mg incorporation. The growth and decay of photocurrent spectra under UV illumination for all the samples annealed at 500 °C is shown in Fig. 8a. The photocurrent spectra of MZO alloy films exhibit a fast rise upon UV illumination. On the other hand, when the UV light is turned off, the decay is relatively slow. The slower decay of the photocurrent is mainly attributed to the formation of trap states at the grain boundaries. The Mg substitution in ZnO brings more ordering among the atoms at the grain boundaries. This leads to a decrease in the decay time with Mg substitution as shown in Fig. 8b. Similar trend has also been observed by Ghosh et al. [30]. But, in the present case, the decay times are found to be one order of magnitude higher than the values reported by Ghosh et al. However, for higher Mg concentration ($x = 0.3$), the decay time is more due to the anomalous change in the surface morphology leading to the creation of more number of defects at the grain boundaries.

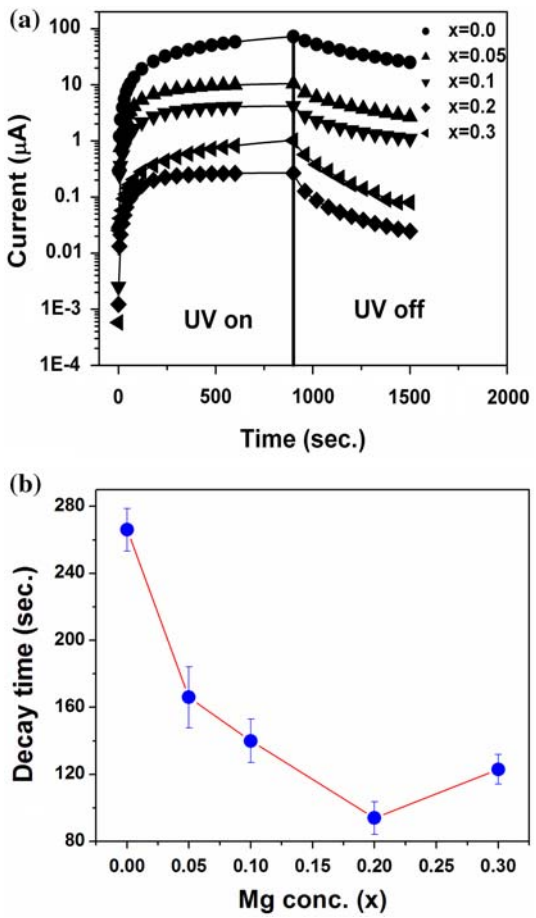

Fig. 8 **a** Photocurrent spectra of MZO films annealed at 500 °C under UV illumination at a biasing voltage of 10 V. **b** Decay time as a function of Mg content in the MZO alloy films

4 Conclusions

In the present study, polycrystalline wurtzite MZO alloy films with different Mg concentrations were prepared by sol–gel method. The band gap of ZnO was successfully tailored from 3.2 to 3.7 eV by alloying it with different Mg concentrations and annealing them at different temperatures. For the films with $x = 0.1$ and 0.2, the band gap at first increased up to a certain critical annealing temperature due to the proper incorporation of Mg atoms into the ZnO lattice points. For the MZO film with $x = 0.3$, the critical annealing temperature was found to be low because of poor bonding of Mg atoms into the alloy film at higher Mg concentration. Furthermore, the band gap values obtained from transmission spectra were found to be in good agreement with the values obtained from PL spectra.

Acknowledgments The authors would like to acknowledge the Sophisticated Analytical Instrumentation Facility (SAIF), IIT Madras for the photoluminescence (PL) measurements.

References

1. Ohtomo A, Kawasaki M, Koida T, Masubuchi K, Koinuma H, Sakurai Y, Yoshida Y, Yasuda T, Segawa Y (1998) Appl Phys Lett 72:2466. doi:10.1063/1.121384
2. Sun HD, Makino T, Segawa Y, Kawasaki M, Ohtomo A, Tamura K, Koinuma H (2001) Appl Phys Lett 78:3385. doi:10.1063/1.1375830
3. Yang Y, Hullavard SS, Nagaraj B, Takeuchi I, Sharma RP, Venkaesan T, Vispute RD, Shen H (2003) Appl Phys Lett 82:3424. doi:10.1063/1.1576309
4. Coli G, Bajaj KK (2000) Appl Phys Lett 78:2861. doi:10.1063/1.1370116
5. Heitsch S, Benndorf G, Zimmermann G, Schulz C, Spemann D, Hochmuth H, Schmidt H, Nobis T, Lorenz M, Grundmann M (2007) Appl Phys A Mater Sci Process 88:99. doi:10.1007/s00339-007-3953-5
6. Park SH, Ahn D (2006) Opt Quantum Electron 38:935. doi:10.1007/s11082-006-9007-y
7. Ohtomo A, Tamura K, Saikusa K (1996) Appl Phys Lett 75:2635. doi:10.1063/1.125102
8. Park WI, Yi GC, Jang HM (2001) Appl Phys Lett 79:2022. doi:10.1063/1.1405811
9. Sun HD, Makino T, Segawa Y, Kawasaki M, Ohtomo A, Tamura K, Koinuma H (2002) J Appl Phys 91:1993. doi:10.1063/1.1445280
10. Minemoto T, Negami T, Nishiwaki S, Takakura H, Hamakawa Y (2000) Thin Solid Films 372:173. doi:10.1016/S0040-6090(00)01009-9
11. Chen NB, Wu HZ, Xu TN (2005) J Appl Phys 97:023515. doi:10.1063/1.1821633
12. Jin YB, Zhang B, Yang SM, Wang YZ, Chen J, Zhang HZ, Huang CH, Qao CQ, Cao H, Chang RPH (2001) Solid State Commun 119:409. doi:10.1016/S0038-1098(01)00244-7
13. Narayan J, Sharma AK, Kvit A, Jin C, Muth JF, Holland OW (2002) Solid State Commun 121:9. doi:10.1016/S0038-1098(01)00431-8
14. Choopun S, Vispute RD, Yang W, Sharma RP, Venkatesan T, Shen H (2002) Appl Phys Lett 80:1529. doi:10.1063/1.1456266
15. Ji Z, Song Y, Xiang Y, Liu K, Wang C, Ye Z (2004) J Cryst Growth 265:537. doi:10.1016/j.jcrysgro.2004.02.083
16. Sarver JF, Katnack FL, Hummel FA (1959) J Electrochem Soc 106:960. doi:10.1149/1.2427190
17. Zhao D, Liu Y, Shen D, Liu Y, Zhang J, Fan X (2001) J Appl Phys 90:5561. doi:10.1063/1.1413948
18. Wang M, Kim EJ, Kim S, Chung JS, Yoo IK, Shin EW, Hahn SH, Park C (2008) Thin Solid Films 516:1124. doi:10.1016/j.tsf.2007.05.039
19. Ghosh R, Basak D (2007) J Mater Sci Mater Electron 18:S141. doi:10.1007/s10854-007-9169-9
20. Kim YII, Page K, Seshadri R (2007) Appl Phys Lett 90:101904. doi:10.1063/1.2711289
21. Keffer F, Portis AM (1957) J Chem Phys 27:675. doi:10.1063/1.1743813
22. Tauc J, Grigorovici R, Vancu A (1966) Phys Status Solidi 15:627. doi:10.1002/pssb.19660150224
23. Ashrafi ABMA, Segawa Y, Shin K, Yao T (2005) Phys Rev B 72:155302. doi:10.1103/PhysRevB.72.155302
24. Brus LE (1984) J Chem Phys 80:4403. doi:10.1063/1.447218
25. Dietz RE, Hopfield JJ, Thomas DG (1961) J Appl Phys 32:2282. doi:10.1063/1.1777060
26. Chen Y, Bagnall DM, Koh HJ, Park KT, Hiraga K, Zhu Z, Yao T (1998) J Appl Phys 84:3912. doi:10.1063/1.368595
27. Ohtomo A, Shiroki R, Ohkubo I, Koinuma H, Kawasaki M (1999) Appl Phys Lett 75:4088. doi:10.1063/1.125545
28. Zhang DH, Xue ZY, Wang QP (2002) J Phys D Appl Phys 35:2837–2840. doi:10.1088/0022-3727/35/21/321
29. Rosenblatt GH, Rowe MW, Williams GP Jr, Williams RT (1989) Phys Rev B 39:10309–10318. doi:10.1103/PhysRevB.39.10309
30. Ghosh R, Basak D (2007) J Appl Phys 101:113111. doi:10.1063/1.2743887